Single-particle localization in dynamical potentials

Jan Major
Instytut Fizyki imienia Mariana Smoluchowskiego, Uniwersytet Jagielloński, Ulica Profesora Stanisława Łojasiewicza 11, PL-30-348 Kraków, Poland

Giovanna Morigi
Theoretische Physik, Universität des Saarlandes, D-66123 Saarbrücken, Germany

Jakub Zakrzewski
Instytut Fizyki imienia Mariana Smoluchowskiego, Uniwersytet Jagielloński, Ulica Profesora Stanisława Łojasiewicza 11, PL-30-348 Kraków, Poland
and Mark Kac Complex Systems Research Center, Uniwersytet Jagielloński, Ulica Profesora Stanisława Łojasiewicza 11, PL-30-348 Kraków, Poland

(Received 27 August 2018; published 28 November 2018)

Single-particle localization of an ultracold atom is studied in one dimension when the atom is confined by an optical lattice and by the incommensurate potential of a high-finesse optical cavity. In the strong-coupling regime the atom is a dynamical refractive medium, the cavity resonance depends on the atomic position within the standing-wave mode, and nonlinearly determines the depth and form of the incommensurate potential. We show that the particular form of the quasirandom cavity potential leads to the appearance of mobility edges, even in presence of nearest-neighbor hopping. We provide a detailed characterization of the system as a function of its parameters and, in particular, of the strength of the atom-cavity coupling, which controls the functional form of the cavity potential. For strong atom-photon coupling the properties of the mobility edges significantly depend on the ratio between the periodicities of the confining optical lattice and of the cavity field.

DOI: 10.1103/PhysRevA.98.053633

I. INTRODUCTION

The Aubry-André model [1] describes a quantum particle tightly confined by a one-dimensional lattice, and in the presence of a second periodic potential, a harmonic function whose period is incommensurate with the main lattice period. In such a system, when the second potential exceeds some critical height all states are exponentially localized, very likely as in the case of Anderson localization in truly disordered systems [2]. The fact that localization indeed manifests in the Aubry-André model has been formally proven in Ref. [3]. Due to its spatial correlations, the Aubry-André potential and its extensions are often referred to as *quasi-disordered* potentials.

Detailed studies of disorder-induced effects are presently possible, since ultracold atomic systems allow an unprecedented level of controllability over the system parameters [4–6]. This is particularly true for optical lattice potentials where different lattice geometries can be realized [7], as on-site potentials as well as tunnelings can be tailored. Moreover, artificial gauge fields can be simulated, often adapting periodic modulations of lattice parameters or interactions [8–17]. Of particular value is the control over the interaction strength by means of Feshbach resonances [18].

Early propositions to study disorder-induced effects in cold atom settings [19,20] soon resulted in experimental attempts to observe direct signatures of localization in interacting condensates [21–25]. Only when interactions were turned off could localization be directly observed in ultracold atomic gases placed in speckle [26] or quasirandom [27] potentials in quasi-one-dimensional (1D) systems. The latter case is precisely the case of Aubry-André localization [1]. Soon afterwards further progress was made, leading to the demonstration of three-dimensional (3D) Anderson localization [28,29]. With the development of many-body localization theory [30,31] it became clear that a sufficiently strong disorder leads also to localization for interacting particles, breaking the common wisdom of ergodicity in such systems [32]. Research on many-body localization has rapidly advanced in recent years (see, e.g., reviews [33,34]), followed by exciting experimental developments [35,36]. While early theoretical work considers spin systems (reducing in some cases to spinless fermions), many-body localization is predicted to occur also for bosons [37–39]. Let us also note that Anderson localization is predicted to occur for solitons, namely, even for weak disorder and in the presence of interactions [40].

Notwithstanding the rising interest in localization in interacting systems, the noninteracting limit is still at the center of intensive studies on the critical dynamics close to the localization transition [41,42]. Moreover, the position of the mobility edge for 3D Anderson localization is a subject of current debate [43,44]. Anderson localization is studied in a variety of systems, and recent propositions suggest that the phenomenon can occur in the time domain [45,46] and it can be understood in terms of time crystals [47–49] (for a review see [50]). The one-dimensional case presents peculiar features. Here, even a tiny truly random disorder leads to

localization of all eigenstates. On the contrary, Aubry-André localization in quasiperiodic potentials occurs at a threshold value. This behavior is modified when hopping in the main lattice has tails beyond nearest-neighbor coupling [51,52]. In this modified Aubry-André model one may observe (as in the standard 3D case) mobility edges, i.e., situations where, for a given disorder, the energy eigenstates within a band can be delocalized or localized and are separated in energy by a "mobility edge" [53]. Similarly, nontrivial correlations in disorder or nondiagonal disorder (e.g., random tunnelings) lead to an appearance of mobility edges [54–64].

In this work we show that mobility edges with peculiar features can appear in a different extension of the Aubry-André model, where the hopping is nearest neighbor and uniform while the incommensurate potential, in turn, is not a simple harmonic function but instead can possess all higher harmonics. This model is an idealization of the dynamics of atoms which are confined by optical lattice potentials and interacts with a standing-wave mode of a high-finesse optical resonator when the system is pumped by a laser which either couples directly to the cavity or pumps the atoms transversally. Here, the strong optomechanical coupling with the atoms gives rise to a shift of the cavity resonance which depends on the atomic density within the cavity standing wave, and thus to a nonlinear dependence of the intracavity potential on the atomic density [65–68]. When the atoms are transversally pumped by the laser and the periodicity of the cavity mode and optical lattice are commensurate, interacting atoms can form density-wave phases [69–72]. Similarly, the incommensurate ratio of these frequencies may lead to a quasirandom potential, giving rise to disordered phases in interacting systems [73,74]. The ground state of a single cold atom for incommensurate ratios was analyzed in Ref. [75]. It was shown that the specific incommensurate potential of the cavity field—compare Eq. (6) below—leads to Anderson-like localization of the ground state. This localization is due to the incommensurate potential which emerges because of cavity backaction and is thus self-induced by the atom. It has been argued that the dynamics of atomic wave packets in a related model can exhibit anomalous diffusion [76]. In this work we significantly extend the previous study of Ref. [75] by analyzing the properties of excited states in the configuration originally proposed in [75]. We show that this model can exhibit a mobility edge. The appearance of a mobility edge depends on the strength of the coupling between the atom and the cavity mode, and results thus from the nonlinear character of the optomechanical potential. Interestingly, the system's behavior exhibits a dramatic dependence on the incommensurability parameter and it is thus sensitive to the quasirandom disorder of the self-induced cavity potential. The paper is structured as follows. In Sec. II we present the model used and we sketch its derivation. In Sec. III we show and discuss the results of the numerical calculations. The conclusions are drawn in Sec. IV.

II. MODEL

In this section we introduce and justify the model which is the starting point of our investigation. The material here presented summarizes the detailed derivations reported in Refs. [67,74,75].

A. Optomechanical coupling between atomic motion and cavity

The system we consider is an atom of mass m whose motion is constrained along one dimension, which we identify here with the x axis. The atomic motion is tightly bound by an optical lattice and confined inside a high-finesse optical resonator, which in turn is driven by a laser. An atomic dipolar transition strongly couples to one standing-wave mode of the resonator which dissipates photons at rate κ. We consider the limit in which the coupling is purely optomechanical, namely, the atomic internal degrees of freedom can be described by the dispersive polarizability, and cavity and atomic motion are directly coupled to one another. The Hamiltonian part of the dynamics takes the form

$$H_{\rm opto} = \frac{p^2}{2m} + W_0 \cos^2(2\pi x/\lambda_0) - \hbar\Delta_c a^\dagger a + i\hbar\eta(a^\dagger - a) + \hbar U_0 a^\dagger a \cos(2\pi x/\lambda)\,, \quad (1)$$

where p and x are the canonically conjugated momentum and position of the atom, W_0 and λ_0 are the depth and wavelength of the optical lattice, respectively, and a and $a^\dagger$ are the annihilation and creation operator of a cavity photon at frequency ω_c and wavelength λ. The parameter η denotes the strength of the pumping laser at frequency ω_p, and the Hamiltonian is reported in the reference frame rotating at the pump frequency, with $\Delta_c = \omega_p - \omega_c$ the detuning between pump and cavity frequency. Finally, the optomechanical coupling between the cavity and atomic motion gives rise to an optical lattice at periodicity λ and depth $U_0 a^\dagger a$. In turn, this term also describes a shift of the cavity frequency which depends on the atomic position, $U_0 \cos(2\pi x/\lambda)$. Therefore, this term gives rise to a nonlinear coupling between atomic motion and resonator, which is scaled by the parameter U_0. In particular, U_0 can be either positive or negative, depending on the sign of the atomic detuning [68].

The incoherent part of the dynamics is solely given by cavity losses and is described by a Born-Markov master equation for the density matrix ρ of the cavity and atom's external degrees of freedom. The full master equation reads

$$\partial_t \rho = \frac{1}{i\hbar}[H_{\rm opto}, \rho] + \mathcal{L}\rho\,, \quad (2)$$

where the dissipator $\mathcal{L}$ describes the cavity losses:

$$\mathcal{L}\rho = \kappa(2a\rho a^\dagger - a^\dagger a\rho - \rho a^\dagger a)\,. \quad (3)$$

Losses due to spontaneous emission are here neglected, since the fields are far off resonance from the optical dipole transition so that the atom-light interactions are in the dispersive regime.

In the rest of this work we will focus on the atomic motion. This is confined by two potentials: the external optical lattice, at fixed depth, and the cavity standing-wave potential, whose depth is proportional to the number of intracavity photons and is thus a dynamical variable. We focus on the dynamics when the ratio β between the two periodicity, $\beta = \lambda_0/\lambda$, is incommensurate. This situation would reproduce the Aubry-André model, but with an important difference due to the optomechanical coupling, which gives rise to an effective nonlinearity in the dynamics of the atomic motion for sufficiently large values of U_0. The parameter U_0, indeed, is

related to the dispersive cooperativity C_0 of cavity quantum electrodynamics [77] by the relation $C_0 = |U_0|/\kappa$. In the regime where $C_0 \geqslant 1$, the backaction of the cavity field on the atomic motion thus appears in terms of a potential which contains higher harmonics than the one at wave number $k = 2\pi/\lambda$. This becomes evident in the limit in which the cavity degrees of freedom can be eliminated from the equations of motion of the atom, which is the regime on which we focus in the rest of this paper.

B. Eliminating the cavity degrees of freedom

We now consider the regime in which the characteristic timescale τ_c of the cavity degrees of freedom is orders of magnitude smaller than the characteristic timescale T_M of the atomic motion. In this regime $\tau_c \sim |\Delta_c + i\kappa|^{-1}$ and $T_M \sim \sqrt{\omega_R E_{\rm kin}}$, where $\omega_R = 2\pi^2/(m\lambda^2)$ is the recoil energy and $E_{\rm kin}$ is the average atom's kinetic energy. For $\sqrt{\kappa^2 + \Delta_c^2} \gg \sqrt{\omega_R E_{\rm kin}}$ we can perform a coarse graining over time Δt, such that $\tau_c \ll \Delta t \ll T_M$. Moreover, for sufficiently large ratios T_M/τ_c the cavity shot noise can be neglected and the field variable can be replaced by its average value over Δt, which is now a function of the atomic variable:

$$a \to \bar{a} \approx \eta/[(\Delta_c - U_0 \cos^2(kx)) + i\kappa]\,.$$

Details of this procedure can be found in Refs. [65,67,73] (see Ref. [78] for the semiclassical approximation). In this limit the dynamics is described by the effective Hamiltonian:

$$H_{\rm eff} = \frac{p^2}{2m} + W_0 \cos^2(\pi x) + \varepsilon(x)\,, \tag{4}$$

where we have now reported the position x in units of $\lambda_0/2$. The term $\varepsilon(x)$ is the nonlinear potential due to cavity backaction, which reads [75]

$$\varepsilon(x) = V_0 \arctan(-\delta + C\cos^2(\beta\pi x))\,,$$

with $V_0 = \hbar\eta^2/\kappa$ a proportionality factor whose strength is controlled by the pump intensity, $\delta = \Delta_c/\kappa$, $C = U_0/\kappa$ (such that $C_0 = |C|$), and β some irrational number. In the first part of this paper we set it equal to the golden ratio $\phi = (1+\sqrt{5})/2$.

The parameter C, which we will denote from now on by "cooperativity," can be both negative and positive, depending on the sign of U_0 and thus of the detuning between fields and atomic transition. This is important for the following discussion, since when $C > 0$ the minima of the cavity potential are at the nodes of the cavity standing wave, and thus where the intracavity intensity vanishes. For $C < 0$, instead, the minima are the maxima of the intracavity intensity.

Finally, for sufficiently deep optical lattices we use the tight-binding and single-band approximation, and obtain a modified Harper's Hamiltonian,

$$H_{\rm TB} = -t\sum_n [|n\rangle\langle n+1| + |n\rangle\langle n-1| + \varepsilon_n |n\rangle\langle n|]\,, \tag{5}$$

where $|n\rangle$ is the state vector for the particle localized on the nth site of the lattice, t is hopping integral, and ε_n scales the on-site energy:

$$\varepsilon_n = V \arctan(-\delta + C\cos^2(\beta\pi n))\,, \tag{6}$$

with $V = V_0/t$ the potential depth in units of the tunneling t. The Hamiltonian (5) has been obtained in the basis of Wannier functions, which are localized on the optical lattice sites, and discarding long-range hopping as well as inhomogeneities in the tunneling coefficients caused by cavity potential $\epsilon(x)$. We remark that, despite that the initial model is driven dissipative, in the regime where we can adiabatic eliminate the cavity degrees of freedom the atomic dynamics is strictly Hamiltonian, and thus different from the model considered in Ref. [76]. The Hamiltonian description of Eq. (4) is valid as long as the coarse-graining discussed above and in Refs. [65,67,73,78] applies.

In the rest of this work we will analyze the spectrum of excitations of the Hamiltonian $H_{\rm TB}$ as a function of V, C, and δ. These parameters have specific physical meanings. The dimensionless potential depth V is proportional to the intensity of the pump, and thus to the average number of intracavity photons. The parameters δ and $|C|$ determine the form of the cavity-induced potential. The cooperativity C determines the strength of the cavity-atom optomechanical coupling. For $|C| \ll 1$ the on-site energy essentially reduces to a single harmonic, however with the new amplitude $V' = |C|V/[2(\delta^2+1)]$ and the shift $-\text{atan}(\delta)$. The critical value at which localization occurs is found at $V' = 2t/\alpha$, with α a factor depending on the overlap integral between the Wannier functions and the incommensurate potential in the harmonic limit [75]. When $|C| \geqslant 1$, instead, higher harmonics become relevant: the value of $|C|$ and its sign determine the form of the nonlinear potential that the atom experiences.

We finally remark that the model of Eq. (4) is strictly valid when only one atom interacts with the cavity field. Thus, it cannot be extended to a Bose-Einstein condensate of atoms with vanishing scattering length, since the atoms will still experience the cavity-mediated long-range interactions [65,67]. Therefore, in this work $C_0 = |C|$ is, strictly speaking, the single-atom cooperativity [77]. Experiments confining a controllable number of atoms within high-finesse optical resonators using a dipole trap have been recently performed, see, for instance, Refs. [79–81].

III. EXCITATION SPECTRUM AND MOBILITY EDGES

The ground-state properties of the system described by the Hamiltonian (5) have been analyzed in detail in Ref. [75]. Due to the fact that the potential contains higher harmonics, the model is not dual. Nevertheless, the ground state exhibits a transition between extended and localized wave function, whose transition point is shifted with respect to the transition without cavity backaction. In particular, for sufficiently large values of $|C|$, in the localized phase the ground-state probability density can exhibit a very small, yet finite, contribution from a constant density offset, while the Lyapunov exponent of the exponentially localized component is a function of the cooperativity.

In this section we analyze the properties of the excited states, focusing in particular on identifying a nontrivial mobility edge, namely, an energy eigenstate separating localized

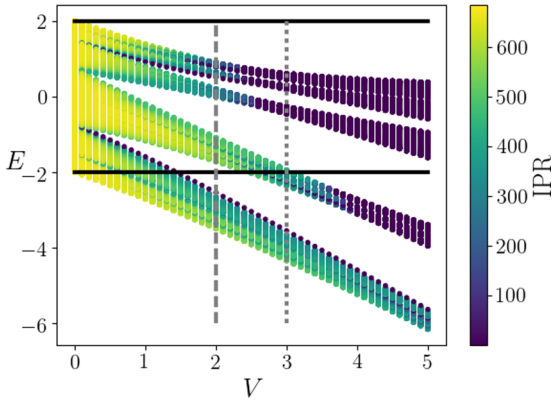

FIG. 1. Eigenenergies (in units of t) as a function of the dimensionless potential depth $V = V_0/t$ for $\beta = \phi$, $C = -2$, and $\delta = 0$. The dots correspond to the energy values, the color (shade of gray in print) represents their IPR as visualized by the bar code. The horizontal black lines indicate the bandwidth for $V = 0$. The gray vertical lines indicate the parameters used in Fig. 5.

and nonlocalized states within a band [82]. To this end we diagonalize the Hamiltonian (5), taking an optical lattice with $N = 1000$ sites and open boundary conditions. Using the eigenstates $\psi_j(n)$, where $\psi_j(n)$ is the value of the j eigenstate at the lattice site n, we determine the inverse participation ratio IPR (see, e.g., [83,84]):

$$\mathrm{IPR}_j = \left(\sum_n |\psi_j(n)|^4 \right)^{-1}. \tag{7}$$

From construction IPR $= 1$ for perfect localization, namely, when only one site is occupied. This is the minimal value it can take. The maximal value IPR $= N$ corresponds to the case of a uniform distribution over the whole lattice. The chosen system size $N = 1000$ is sufficiently large to clearly distinguish between extended states, whose IPR is of order of several hundreds, and localized states. We checked that states with IPR values about 10–20 are exponentially localized. Our calculations show that nearly all eigenstates have IPR which falls into one of these ranges of values. An example of the energy spectrum as a function of V is shown in Fig. 1 for $C = -2$ and $\delta = 0$. The dots correspond to the energy values, and the color (shade of gray) represents their IPR. One can observe the abrupt change of the IPR from large to low values (where IPR ~ 10). Moreover, the states of a whole subband become localized or extended nearly for the same value of V.

The presence of mobility edges can be visualized by introducing the new parameter R, which is the ratio between the number of localized states (here, states with IPR < 50) over N and is defined as

$$R = \frac{\#(\mathrm{IPR} < 50)}{N}, \tag{8}$$

where the threshold IPR $= 50$ has been identified for a lattice of $N = 1000$ sites. The ratio R can take all values between 0 and 1, where $R = 0$ corresponds to the situation in which all states are extended while for $R = 1$ all states are localized. Thus an abrupt transition between the extreme values of R indicates the localization transition for all the states. Instead,

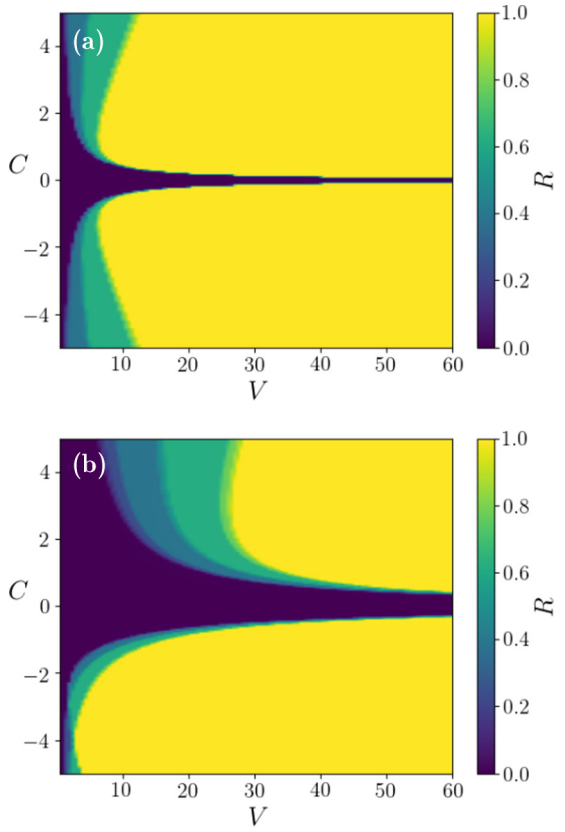

FIG. 2. Contour plot of the ratio of localized states R, Eq. (8), as a function of the dimensionless potential depth V and of the cooperativity C for $\beta = \phi = (1 + \sqrt{5})/2$ and offsets (a) $\delta = 0$ and (b) $\delta = -2$ [see Eq. (6)].

a gradual change of R points towards the existence of the mobility edge, where for given parameter values only part of the eigenstates is localized.

Figure 2 displays R as a function of the on-site disorder parameters V and C for $\delta = \{0, -2\}$ in Eq. (6). For very small $|C|$, as expected, all states are extended with vanishing R, at least at the range of V considered. For stronger cooperativity C, the localization sets in, but the border between the $R = 0$ and $R = 1$ regime is smeared out over a significant range of V values. In the region corresponding to intermediate R values only a fraction of states reveals localization. Thus, some of the eigenstates of the system for say, $C \approx 4$, $V \approx 8$ are localized while others are extended. Since localized and delocalized states cannot coexist at similar energies, this behavior indicates the existence of the mobility edge in energies.

A further insight may be gained in comparing Fig. 2(a) with Fig. 2(b) of Ref. [75]. In the latter the participation ratio, i.e., the inverse of (7), is plotted (accidentally, it is called there an inverse participation ratio, in obvious contradiction with the IPR definition [83,84]) for the *ground* state of the system. As expected, the localization border for the ground state is sharp. For positive C it corresponds to the smaller V border of the transition region in Fig. 2(a). Thus for parameters in this region (e.g., $C \approx 4$, $V \approx 8$), the ground state is already localized while some excited states are still extended. This proves the existence of the mobility edge in the system,

separating the low-lying localized states from the higher-lying extended states in this transition regime.

In this way we can convince ourselves about the existence of a single mobility edge. It may be possible that there exists also an upper mobility edge not revealed by comparison with the ground-state properties. Its detection would require a detailed study of R as a function of the energy, which is beyond the scope of the present paper. Let us note, however, that the mobility edge becomes "inverted" for negative C. Here, in the parameter regime where R already takes intermediate values, the ground state may remain extended (as visible by comparing Fig. 2(a) with Fig. 2(b) of Ref. [75]), thus suggesting localization of some excited states.

For $\delta = -2$ [Fig. 2(b)], we observe the similar behavior as for $\delta = 0$ with a large transition region but only for positive C values. For $C < 0$ the interval of V values where the mobility edge is found shrinks at $C \sim -4$. We note that for the same parameters this is the region where bistability is expected for interacting atoms in the same setup [85]. In general, the variation of R with V occurs in steps. This is a consequence of the fact that the energy band splits into flat subbands by increasing V from zero, as visible in Fig. 1.

So far we discussed the mobility edge for an incommensurability ratio equal to the golden mean, $\beta = \phi = (\sqrt{5}+1)/2$, which is traditionally used in most of the studies in the field. The proof of the localization in the Aubry-André model given in Ref. [3] is derived for any diophantic number—the number "as much incommensurate" as a golden ratio—having the same expansion into a continuous fraction from some point. We will now verify whether any diophantic number gives the same results for the potential we are considering, Eq. (6). For this purpose we use the formula

$$\phi_{cd}^{ab} = \frac{a + b\phi}{c + d\phi}, \tag{9}$$

which delivers a whole (infinite, countable) family of diophantic numbers when a, b, c, and d are integers fulfilling the relation $ad - bc = \pm 1$, and $\phi = (1+\sqrt{5})/2$ is the golden ratio [86]. We construct a set of diophantic numbers ϕ_{cd}^{ab} in the following way. We take $\ell \in \{2, \ldots, 15\}$. For each ℓ we find the set of all divisors of ℓ, $D = D_1, \ldots$, and of $\ell - 1$, $D' = D'_1, \ldots$. Then we construct the subsequent ϕ_{cd}^{ab}'s by taking $a = D_i$, $b = D'_j$, $c = (\ell-1)/D'_j$, and $d = \ell/D_i$, and by eliminating reappearing configurations. This yields a set of $M = 122$ diophantic numbers ϕ_{cd}^{ab}. We then evaluate $R(\beta)$ for each value of $\beta = \phi_{cd}^{ab}$ from this set and determine the average $\langle R\rangle_{\{\beta\}}$ and its standard deviation $\sigma(R)_{\{\beta\}}$, defined as

$$\langle R\rangle_{\{\beta\}} = \frac{1}{M}\sum_{\beta} R(\beta), \tag{10}$$

$$\sigma(R)_{\{\beta\}} = \sqrt{\langle R^2\rangle - \langle R\rangle^2}. \tag{11}$$

The mean $\langle R\rangle_{\{\beta\}}$ is shown in the top panels of Figs. 3 and 4 as a function of V and C for two different δ values. A comparison of the mean plots with Fig. 2 shows that the parameter regions corresponding to all the states being extended or being localized is not sensitive to changes of the incommensurate ratio. (Note that the horizontal scale is smaller in Figs. 3 and 4 than in Fig. 2 for better visibility of the details of the transition region.) On the other hand, the contours of the intermediate regime, where the mobility edge appears, are smoothened. This indicates that the position of the mobility edge depends on the specific incommensurability ratio. To our knowledge, this feature has not been reported in other extensions of the Aubry-André model before.

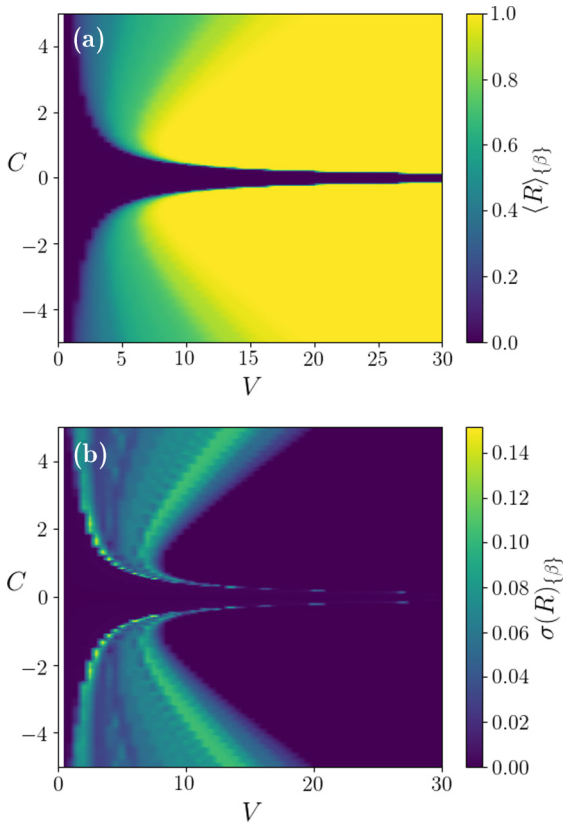

FIG. 3. Contour plots of (a) the average ratio of localized states $\langle R\rangle$, Eq. (10), and (b) the standard deviation $\sigma(R)$ of the distribution, Eq. (11), as a function of C and V for offset $\delta = 0$ in the potential of Eq. (6). The average is taken over 122 different values of diophantic numbers $\beta = \phi_{cd}^{ab}$ (see text for details).

To see whether this effect is really important, let us consider the standard deviation $\sigma(R)_{\{\beta\}}$ of R distribution shown in the lower panels in Figs. 3 and 4. Clearly, deep in the localized regime (where $R \approx 1$) and in the extended regime (where $R \approx 0$) also the standard deviation takes very small values. By comparison, $\sigma(R)_{\{\beta\}}$ is significant in the transition regime between extended and localized states. Thus, indeed, in this regime the behavior of the system is sensitive to the incommensurability ratio.

Let us mention, finally, that the existence of controlled mobility edges could be utilized for a transportlike experiment, in the spirit of the proposal in Ref. [59] where Anderson localization in a spatially correlated disorder potential is shown to operate as a bandpass filter, which selects atoms with certain momenta. In order to show these dynamics in our system, we simulate the time evolution in our model assuming that the atom initially occupies a single site at the center of the system. We assume a quasiperiodic lattice of 100 sites, surrounded by two "empty" regions on both sides, both consisting of

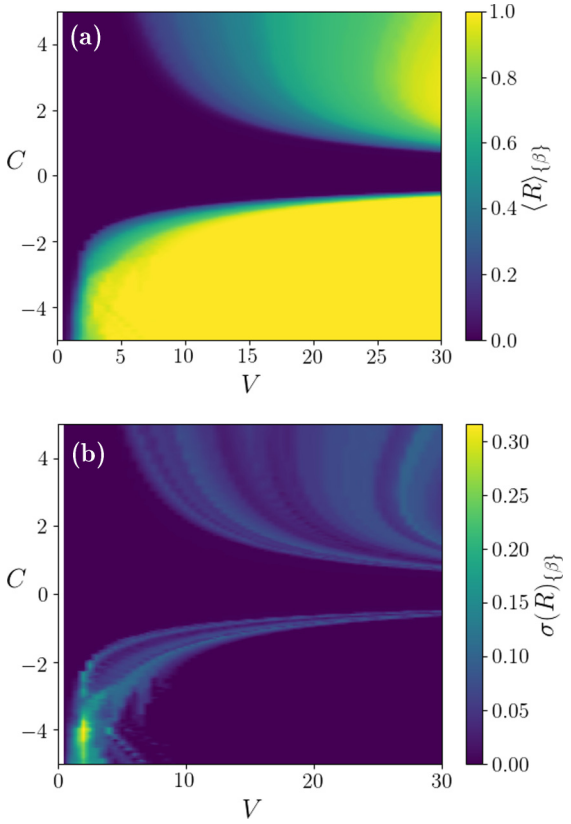

FIG. 4. Same as Fig. 3 but for the offset parameter $\delta = -2$ in the potential of Eq. (6).

500 sites. The size of the central region is chosen to exceed the localization length. The numerical evolution is calculated using a fourth-order Adams predictor-corrector method up to time $T = 400/t$. This time duration is sufficiently long to allow for the extended component of the initial wave function to leave the central region. In order to obtain the distribution of momenta $\psi(k)$ of waves that managed to escape from the central region, we set to zero the part of the wave function localized in the central region and take the Fourier transform of the remaining part. Figure 5 displays $|\psi(k)|^2$ as a function of k at time T. It can be seen that by manipulating the system parameters one can select waves within a certain window of momenta, making it possible to use this class of systems as filters for momenta of particles [59]. We do not have an analytical description in this case (as is possible for some classes of disordered potentials [64]). On the other hand, the advantage of the system presented here lies in the fact that the disorder is quasirandom and, therefore, may be reproducible.

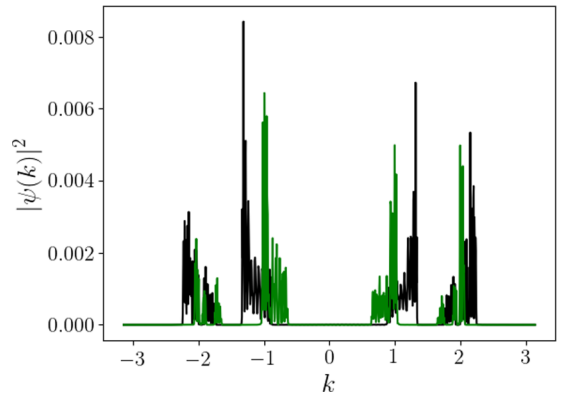

FIG. 5. Distribution $|\psi(k)|^2$ of momenta of waves, leaving the central quasidisordered region of the system, as a function of k. The distribution is evaluated numerically after evolving an initially localized wave function for a time $T = 400/t$. The parameters are $\delta = 0$, $C = -2$, while $V = 2$ and $V = 3$ for black and green lines, respectively. The atom is initially at the center of the quasidisordered potential. See text for further details.

IV. CONCLUSIONS

Starting from the model proposed in [75], we have given a description of the localization properties by determining the full spectrum as a function of the system parameters. We have shown that there exists a finite range of parameters where a mobility edge exists—some states are localized while other remain extended. We have also shown that fully localized or fully extended states exist in regions of the parameters space and that these regions are quite robust upon changing the incommensurability ratio β. Yet, the region where the mobility edge exists is strongly influenced by the value of β, even if this is any other diophantic number than the golden ratio. In particular, both the position of the mobility edge in parameter space, as well as the fraction of localized states, strongly depend on the chosen incommensurability ratio β as revealed by a significant variance of this fraction when different incommensurate parameters are taken. Finally, we have discussed a possible application of the sensitivity on β as a filter for the momenta of ultracold atoms.

We note that the localization properties physically originate from the backaction of the cavity field on the atom. The field leaking at the cavity mirrors, moreover, contain information about the atomic state and dynamical properties; this property has been successfully applied, for instance, for measuring Bloch oscillations [87–89]. Future work will focus on the characterization of coherence properties of the emitted light in order to identify and monitor the localization properties.

Note added. After finishing this work we became aware of a recent preprint [90] discussing mobility edges for other types of incommensurate lattice potentials.

ACKNOWLEDGMENTS

The authors thank T. Fogarty, A. Minguzzi, K. Rojan, and especially Hessam Habibian and Rebecca Kraus, for discussions. J.M. and J.Z. acknowledge support by the National Science Centre, Poland, via projects OPUS: 2016/21/B/ST2/01086 and QTFLAG: 2017/25/Z/ST2/03029. Support by the PL-Grid Infrastructure, by the EU via project QUIC (H2020-FETPROACT-2014 No. 641122), by the DFG DACH project ("Quantum Crystals of Matter and Light"), and by the Quantera network "NAQUAS" is also acknowledged. Project NAQUAS has received funding from the QuantERA ERA-NET Cofund in Quantum Technologies implemented within the European Union's Horizon 2020 Programme.

[1] S. Aubry and G. André, Ann. Israel Phys. Soc. **3**, 133 (1980).
[2] P. Anderson, Phys. Rev. **109**, 1492 (1958).
[3] S. Y. Jitomirskaya, Ann. Math. **150**, 1159 (1999).
[4] I. Bloch, J. Dalibard, and W. Zwerger, Rev. Mod. Phys. **80**, 885 (2008).
[5] D. Jaksch and P. Zoller, Ann. Phys. **315**, 52 (2005).
[6] M. Lewenstein, A. Sanpera, and V. Ahufinger, *Ultracold Atoms in Optical Lattices: Simulating Many-Body Quantum Systems* (Oxford University Press, Oxford, 2012).
[7] P. Windpassinger and K. Sengstock, Rep. Prog. Phys. **76**, 086401 (2013).
[8] A. Eckardt, C. Weiss, and M. Holthaus, Phys. Rev. Lett. **95**, 260404 (2005).
[9] H. Lignier, C. Sias, D. Ciampini, Y. Singh, A. Zenesini, O. Morsch, and E. Arimondo, Phys. Rev. Lett. **99**, 220403 (2007).
[10] J. Struck, C. Ölschläger, M. Weinberg, P. Hauke, J. Simonet, A. Eckardt, M. Lewenstein, K. Sengstock, and P. Windpassinger, Phys. Rev. Lett. **108**, 225304 (2012).
[11] K. Sacha, K. Targońska, and J. Zakrzewski, Phys. Rev. A **85**, 053613 (2012).
[12] A. Eckardt, P. Hauke, P. Soltan-Panahi, C. Becker, K. Sengstock, and M. Lewenstein, Europhys. Lett. **89**, 10010 (2010).
[13] A. Rapp, X. Deng, and L. Santos, Phys. Rev. Lett. **109**, 203005 (2012).
[14] A. Przysiężna, O. Dutta, and J. Zakrzewski, New J. Phys. **17**, 013018 (2015).
[15] O. Dutta, M. Gajda, P. Hauke, M. Lewenstein, D.-S. Lühmann, B. A. Malomed, T. Sowiński, and J. Zakrzewski, Rep. Prog. Phys. **78**, 066001 (2015).
[16] J. Major, M. Płodzień, O. Dutta, and J. Zakrzewski, Phys. Rev. A **96**, 033620 (2017).
[17] O. Dutta, L. Tagliacozzo, M. Lewenstein, and J. Zakrzewski, Phys. Rev. A **95**, 053608 (2017).
[18] C. Chin, R. Grimm, P. Julienne, and E. Tiesinga, Rev. Mod. Phys. **82**, 1225 (2010).
[19] B. Damski, J. Zakrzewski, L. Santos, P. Zoller, and M. Lewenstein, Phys. Rev. Lett. **91**, 080403 (2003).
[20] R. Roth and K. Burnett, J. Opt. B **5**, S50 (2003).
[21] J. E. Lye, L. Fallani, M. Modugno, D. S. Wiersma, C. Fort, and M. Inguscio, Phys. Rev. Lett. **95**, 070401 (2005).
[22] D. Clément, A. F. Varón, M. Hugbart, J. A. Retter, P. Bouyer, L. Sanchez-Palencia, D. M. Gangardt, G. V. Shlyapnikov, and A. Aspect, Phys. Rev. Lett. **95**, 170409 (2005).
[23] C. Fort, L. Fallani, V. Guarrera, J. E. Lye, M. Modugno, D. S. Wiersma, and M. Inguscio, Phys. Rev. Lett. **95**, 170410 (2005).
[24] T. Schulte, S. Drenkelforth, J. Kruse, W. Ertmer, J. Arlt, K. Sacha, J. Zakrzewski, and M. Lewenstein, Phys. Rev. Lett. **95**, 170411 (2005).
[25] T. Schulte, S. Drenkelforth, J. Kruse, R. Tiemeyer, K. Sacha, J. Zakrzewski, M. Lewenstein, W. Ertmer, and J. J. Arlt, New J. Phys. **8**, 230 (2006).
[26] J. Billy, V. Josse, Z. Zuo, A. Bernard, B. Hambrecht, P. Lugan, D. Clément, L. Sanchez-Palencia, P. Bouyer, and A. Aspect, Nature (London) **453**, 891 (2008).
[27] G. Roati, C. D'Errico, L. Fallani, M. Fattori, C. For, M. Zaccanti, G. Modugno, M. Modugno, and M. Inguscio, Nature (London) **453**, 895 (2008).
[28] S. S. Kondov, W. R. McGehee, J. J. Zirbel, and B. DeMarco, Science **334**, 66 (2011).
[29] F. Jendrzejewski, A. Bernard, K. Mueller, C. Patrick, V. Josse, M. Piraud, L. Pezze, L. Sanchez-Palencia, A. Aspect, and P. Bouyer, Nat. Phys. **8**, 398 (2012).
[30] D. Basko, I. Aleiner, and B. Altschuler, Ann. Phys. (NY) **321**, 1126 (2006).
[31] V. Oganesyan and D. A. Huse, Phys. Rev. B **75**, 155111 (2007).
[32] M. Srednicki, Phys. Rev. E **50**, 888 (1994).
[33] D. A. Huse, R. Nandkishore, and V. Oganesyan, Phys. Rev. B **90**, 174202 (2014).
[34] R. Nandkishore and D. A. Huse, Annu. Rev. Condens. Matter Phys. **6**, 15 (2015).
[35] M. Schreiber, S. S. Hodgman, P. Bordia, H. P. Lüschen, M. H. Fischer, R. Vosk, E. Altman, U. Schneider, and I. Bloch, Science **349**, 842 (2015).
[36] J.-y. Choi, S. Hild, J. Zeiher, P. Schauß, A. Rubio-Abadal, T. Yefsah, V. Khemani, D. A. Huse, I. Bloch, and C. Gross, Science **352**, 1547 (2016).
[37] P. Sierant, D. Delande, and J. Zakrzewski, Phys. Rev. A **95**, 021601(R) (2017).
[38] P. Sierant, D. Delande, and J. Zakrzewski, Acta Phys. Pol., A **132**, 1707 (2017).
[39] P. Sierant and J. Zakrzewski, New J. Phys. **20**, 043032 (2018).
[40] K. Sacha, C. A. Müller, D. Delande, and J. Zakrzewski, Phys. Rev. Lett. **103**, 210402 (2009).
[41] F. Evers and A. D. Mirlin, Rev. Mod. Phys. **80**, 1355 (2008).
[42] C. A. Müller, D. Delande, and B. Shapiro, Phys. Rev. A **94**, 033615 (2016).
[43] G. Semeghini, M. Landini, P. Castilho, S. Roy, G. Spagnolli, A. Trenkwalder, M. Fattori, M. Inguscio, and G. Modugno, Nat. Phys. **11**, 554 (2015).
[44] M. Pasek, G. Orso, and D. Delande, Phys. Rev. Lett. **118**, 170403 (2017).
[45] K. Sacha and D. Delande, Phys. Rev. A **94**, 023633 (2016).
[46] D. Delande, L. Morales-Molina, and K. Sacha, Phys. Rev. Lett. **119**, 230404 (2017).
[47] F. Wilczek, Phys. Rev. Lett. **109**, 160401 (2012).
[48] K. Sacha, Phys. Rev. A **91**, 033617 (2015).
[49] K. Giergiel, A. Miroszewski, and K. Sacha, Phys. Rev. Lett. **120**, 140401 (2018).
[50] K. Sacha and J. Zakrzewski, Rep. Prog. Phys. **81**, 016401 (2018).
[51] J. Biddle, D. J. Priour, Jr., B. Wang, and S. Das Sarma, Phys. Rev. B **83**, 075105 (2011).
[52] X. Deng, S. Ray, S. Sinha, G. S. Shlyapnikov, and L. Santos, arXiv:1808.03585.
[53] H. P. Lüschen, S. Scherg, T. Kohlert, M. Schreiber, P. Bordia, X. Li, S. Das Sarma, and I. Bloch, Phys. Rev. Lett. **120**, 160404 (2018).
[54] J. Flores, J. Phys.: Condens. Matter **1**, 8471 (1989).
[55] F. Izrailev, Phys. E (Amsterdam, Neth.) **9**, 405 (2001).
[56] R. W. Peng, Y. M. Liu, X. Q. Huang, F. Qiu, M. Wang, A. Hu, S. S. Jiang, D. Feng, L. Z. Ouyang, and J. Zou, Phys. Rev. B **69**, 165109 (2004).
[57] E. Kogan, Eur. Phys. J. B **61**, 181 (2008).
[58] J.-F. Schaff, Z. Akdeniz, and P. Vignolo, Phys. Rev. A **81**, 041604(R) (2010).

[59] M. Płodzień and K. Sacha, Phys. Rev. A **84**, 023624 (2011).
[60] G. Wang, N. Li, and T. Nakayama, arXiv:1312.0844.
[61] A. Kosior, J. Major, M. Płodzień, and J. Zakrzewski, Phys. Rev. A **92**, 023606 (2015).
[62] A. Kosior, J. Major, M. Płodzień, and J. Zakrzewski, Acta. Phys. Pol. A **128**, 1002 (2015).
[63] T. Liu, P. Wang, and G. Xianlong, arXiv:1609.06939.
[64] J. Major, Phys. Rev. A **94**, 053613 (2016).
[65] J. Larson, B. Damski, G. Morigi, and M. Lewenstein, Phys. Rev. Lett. **100**, 050401 (2008).
[66] K. Baumann, C. Guerlin, F. Brennecke, and T. Esslinger, Nature (London) **464**, 1301 (2010).
[67] S. Fernández-Vidal, G. De Chiara, J. Larson, and G. Morigi, Phys. Rev. A **81**, 043407 (2010).
[68] H. Ritsch, P. Domokos, F. Brennecke, and T. Esslinger, Rev. Mod. Phys. **85**, 553 (2013).
[69] J. Klinder, H. Keßler, M. R. Bakhtiari, M. Thorwart, and A. Hemmerich, Phys. Rev. Lett. **115**, 230403 (2015).
[70] R. Landig, L. Hruby, N. Dogra, M. Landini, R. Mottl, T. Donner, and T. Esslinger, Nature (London) **532**, 476 (2016).
[71] N. Dogra, F. Brennecke, S. D. Huber, and T. Donner, Phys. Rev. A **94**, 023632 (2016).
[72] A. E. Niederle, G. Morigi, and H. Rieger, Phys. Rev. A **94**, 033607 (2016).
[73] H. Habibian, A. Winter, S. Paganelli, H. Rieger, and G. Morigi, Phys. Rev. Lett. **110**, 075304 (2013).
[74] H. Habibian, A. Winter, S. Paganelli, H. Rieger, and G. Morigi, Phys. Rev. A **88**, 043618 (2013).
[75] K. Rojan, R. Kraus, T. Fogarty, H. Habibian, A. Minguzzi, and G. Morigi, Phys. Rev. A **94**, 013839 (2016).
[76] W. Zheng and N. R. Cooper, Phys. Rev. A **97**, 021601 (2018).
[77] J. Kimble, in *Cavity Quantum Electrodynamics*, edited by P. R. Berman (Academic Press, New York, 1994), p. 203.
[78] S. Schütz, H. Habibian, and G. Morigi, Phys. Rev. A **88**, 033427 (2013).
[79] R. Miller, T. E. Northup, K. M. Birnbaum, A. Boca, A. D. Boozer, and H. J. Kimble, Phys. E (Amsterdam, Neth.) **38**, S551 (2005).
[80] R. Reimann, W. Alt, T. Kampschulte, T. Macha, L. Ratschbacher, N. Thau, S. Yoon, and D. Meschede, Phys. Rev. Lett. **114**, 023601 (2015).
[81] A. Neuzner, M. Körber, O. Morin, S. Ritter, and G. Rempe, Nat. Photon. **10**, 303 (2016).
[82] N. Mott, J. Phys. C **20**, 3075 (1987).
[83] D. J. Thouless, Phys. Rep. **13**, 93 (1974).
[84] A. Kramer and B. MacKinnon, Rep. Prog. Phys. **56**, 1469 (1993).
[85] T. Fogarty, C. Cormick, H. Landa, V. M. Stojanović, E. Demler, and G. Morigi, Phys. Rev. Lett. **115**, 233602 (2015).
[86] A. Hurwitz, Math. Ann. **39**, 279 (1891).
[87] B. Prasanna Venkatesh, M. Trupke, E. A. Hinds, and D. H. J. O'Dell, Phys. Rev. A **80**, 063834 (2009).
[88] B. P. Venkatesh and D. H. J. O'Dell, Phys. Rev. A **88**, 013848 (2013).
[89] C. Georges, J. Vargas, H. Keßler, J. Klinder, and A. Hemmerich, Phys. Rev. A **96**, 063615 (2017).
[90] X. Li and S. Das Sarma, arXiv:1808.05954.